Journal of Power Sources 241 (2013) 288–294

Contents lists available at SciVerse ScienceDirect

Journal of Power Sources

journal homepage: www.elsevier.com/locate/jpowsour

Tuning pore structure of the poly(vinylidene difluoride hexafluoropropylene) membrane for improvement in rate performance of Li–oxygen battery

Yuan Li [a,b], Yong Yin [a], Kun Guo [a,b], Xinzhong Xue [a], Zhiqing Zou [a], Xuemei Li [a], Tao He [a], Hui Yang [a,*]

[a] Shanghai Advanced Research Institute, Chinese Academy of Sciences, 99, Haike Road, Zhangjiang, PuDong, Shanghai 201210, China
[b] University of Chinese Academy of Sciences, Beijing 100039, China

HIGHLIGHTS

- PVDF-HFP membrane with tuned pore structure is used as a separator for Li–O_2 battery.
- The Li–O_2 battery with PVDF-HFP membrane exhibits an enhanced rate performance.
- Discharge capacity of Li–O_2 battery increases with the pore size of the PVDF-HFP.
- The improved rate performance is due to a faster Li^+ transport across the membrane.

ARTICLE INFO

Article history:
Received 19 January 2013
Received in revised form
23 April 2013
Accepted 25 April 2013
Available online 2 May 2013

Keywords:
Lithium–oxygen battery
Poly(vinylidene difluoride hexafluoropropylene) membrane
Pore structure
Rate performance

ABSTRACT

In this work, the poly(vinylidene difluoride hexafluoropropylene) (PVdF-HFP) membranes with tuned pore structure are prepared and used as a separator for the lithium–oxygen battery. Both oxygen and argon plasma treatments are used to tune the surface pore size and density of the membrane. The discharge capacity of the Li–O_2 battery increases with the pore size and density of the membrane, nearly maximal capacity is achieved with a pore size of ca. 1.48 μm. More importantly, the Li–O_2 battery using the PVdF-HFP membrane with tuned pore structure exhibits a significantly enhanced rate performance, probably due to a faster Li^+ ion transport across the membrane. The highest discharge capacity of 466.1 mAh g^{-1} is achieved at a current density of 5 mA cm^{-2} for the Li–O_2 battery with the PVdF-HFP thickness of 110 μm and pore size of 1.48 μm. Such a discharge capacity is about 10 times higher than that using commercial PP/PE/PP membrane. To our knowledge, it is the first report that the regulation of the pore structure of separator could significantly improve the rate performance of the Li–O_2 battery, which probably provides a new way to solve the low rate characteristics for non-aqueous Li–O_2 battery.

© 2013 Elsevier B.V. All rights reserved.

1. Introduction

Lithium–air (lithium–oxygen) batteries have attracted much attention and are expected to be widely applied in the power system for future electric vehicles because of their high energy density and low cost. Extensive efforts have been made to improve the performance of the lithium–oxygen batteries with respect to cyclability [1–6], charge/discharge efficiency [2,7–10], rate performance [3,11,12] and safety [13], among which, the rate performance is critical in determining the applicability of the Li–O_2 batteries.

The rate performance of the Li–O_2 battery is related to the working current density. Most of the work reported a typical working current density of 0.05–0.25 mA cm^{-2} or 70–200 mA g^{-1}, which was too low to meet the requirements for practical application. To our knowledge, the rate performance of the Li–O_2 battery is closely related to the electrocatalytic activity of the bifunctional electrocatalysts, the specific surface area and pore volume of the cathode and the mass transport rate of both Li^+ ions and O_2. Many reports focused on the use of different materials as the oxygen electrodes [14–16] or exploration of new electrolytes [11,17,18] to improve the rate performance of the Li–O_2 batteries. However, little work has focused on the effect of the pore structure of the separator membrane on the rate performance of the Li–O_2 battery. A copolymer of vinylidene fluoride hexafluoropropylene (PVdF-HFP) has been employed to substitute for the commonly used Celgard membrane and/or Glass

* Corresponding author. Tel./fax: +86 21 20321112.
E-mail addresses: yangh@sari.ac.cn, huiyang65@hotmail.com (H. Yang).

0378-7753/$ – see front matter © 2013 Elsevier B.V. All rights reserved.
http://dx.doi.org/10.1016/j.jpowsour.2013.04.123

fiber filter paper as the separator material for rechargeable lithium batteries due to its good electrochemical stability, electrolyte adsorption and high conductivity. Moreover, the amorphous domains in PVdF-HFP are capable of trapping large amounts of liquid electrolytes, whereas the crystalline regions provided sufficient mechanical integrity [19]. In addition, it is commonly accepted that the material of the separator and its pore structure could have a significant effect on Li^+ ion transport across the separator, and thus the rate performance of the Li–O_2 battery. However, most research works reported the use of commercial membranes as the separator [11,20,21], and making it difficult to investigate the membrane structure effect on the battery performance. Herein, we report the use of tailor-made PVdF-HFP membranes as separators for the Li–O_2 battery with tunable pore structure. The relationship between the pore structure of the PVdF-HFP membrane and the rate performance of the Li–O_2 battery is investigated in order to elucidate the membrane pore structure effect on performance of the Li–O_2 batteries.

2. Experimental section

2.1. PVdF-HFP membrane preparation

The PVdF-HFP was dissolved in a mixture of dimethylacetamide (DMAC) and non-solvent diethylene glycol at certain ratio. The polymer concentration was maintained at 18 wt%. After deaeration, the solution was cast onto a clean dry glass plate. The solution film was immediately immersed in deionized water bath for solidification. The time allowed for transferring the glass plate into the water bath was about 2–3 s. The ambient relative humidity was 50 ± 5%. The membranes were cleaned in water before further treatment with anhydrous ethanol to remove residual solvent. Final membrane was dried for 24 h at room temperature.

Plasma treatment was performed on a plasma system provided by PVA TePla Co. Ltd. The membranes were placed on the plate of the plasma chamber. The system was evacuated to 100 mTorr. Then oxygen gas was injected separately at a rate of 250 standard cubic centimeters (SCCM) with a glow discharge at 300 W for different time (5–15 min). At last the membranes were treated with Ar-plasma by 45 W for 10 min.

2.2. Assembly of the Li–O_2 batteries

The air electrode was prepared as follows. Carbon paper (TGP-H-060, E-TEK Inc.) was used as the current collector and the gas diffusion layer of the air electrode. Ink slurries were prepared by dissolving 80 wt% Ketjen black EC600JD (KB) and 20 wt% PTFE as the binder in isopropyl alcohol and dispersed by mechanical stirring and sonication. Then, the ink slurry was spread layer by layer by hand-painting onto the carbon paper with a loading of 1.5 ± 0.2 mg cm^{-2}. The air electrode was then dried at 60 °C under vacuum for 12 h.

The Li–O_2 batteries were assembled in an argon-filled glove box. The battery consists of metallic lithium foil and the aforementioned air electrode. A polypropylene (PP)/polyethylene (PE)/polypropylene (PP) composite membrane (Celgard 2300, short as PP/PE/PP) separator or a PVdF-HFP membrane separator was inserted between the anode and air electrode. The membranes were soaked in 1 M $LiPF_6$ in EC/DMC (1:1) solution for 12 h. A Swagelok cell with an air hole of 10 mm in diameter was used. The battery was placed in an oxygen-filled bottle where oxygen pressure was maintained around 1 atm.

2.3. Characterizations

Surface morphology of the PVdF-HFP membrane was characterized by Hitachi S-4800 scanning electron microscope (SEM).

Pore size analysis was conducted by capillary flow porometry (Porolux 1000, IB-FT GmbH Berlin, Germany). The membrane was pre-wetted with commercial low surface tension liquid Porewick (surface tension of 16 dyn cm^{-1} based on the supplier's datasheet). The measurement consists of a wet-run program and a dry run program. Membrane pore size was determined by commercial software from Porometer based on Young–Laplace equation:

$$\Delta p = \frac{2\sigma \cos\theta}{r}$$

where Δp, σ, θ and r are the pressure difference, surface tension, contact angle and membrane pore size, respectively.

Absorbency of the membranes was calculated as below:

$$\text{Absorbency}(\%) = (m_2 - m_1)*100/m_1$$

where m_1 refers to the weight of dry PVdF-HFP membrane, m_2 stands for its weight after immersion in the electrolyte for 12 h and wiping the surface liquid in glove box.

The performance of the Li–O_2 batteries was evaluated using a LAND test system (Wuhan Land Electronic Co. Ltd., China) with a lower voltage limit of 2.0 V and a higher voltage limit of 4.5 V. The capacity is normalized to the total mass of the cathode except the current collector.

Electrochemical impedance spectra (EIS) were obtained using a frequency response analyzer (Solartron SI1255B) coupled to a potentiostat/galvanostat (EG&G Model 273A). The ionic conductivities of the composite electrolytes (with membrane and electrolyte) were measured by a.c. impedance with a stainless steel blocking cell at room temperature. For blocking electrodes system, the intersection of impedance spectrum in the high frequency region with real axis stands for the composite electrolyte resistance (R_b). Thus, the ionic conductivity (σ) can be calculated from the electrolyte resistance, film thickness (l) and electrode area (S) using an equation: $\sigma = l/(S\,R_b)$. Impedance measurement was conducted at an open-circuit condition in the frequency range of 0.1 Hz–100 kHz, with an amplitude of 10 mV. The resultant impedance spectra were analyzed based on an electrical circuit element model. The Zview software was used to fit the experimental data to the equivalent circuit.

The lithium ion transport number of the symmetrical cell Li/composite electrolyte/Li was measured by the combination of DC polarization and EIS according to equation: $t^+_{Li} = I_{ss}(\Delta V - I_0R_0)/I_0(\Delta V - I_{ss}R_{ss})$, wherein, I_0 and I_{ss} are the initial and steady current, respectively; R_0 and R_{ss} are the initial interfacial and steady-state resistance, respectively; ΔV is the potential difference.

3. Results and discussion

It is known that the material of the separator and its pore structure could have a significant effect on Li^+ ion transport across the separator, and thus the rate performance of the Li–O_2 battery. In this work, the PVdF-HFP membrane is used as the separator. To explore the possible effect of the separator structure on the performance of the Li–O_2 battery, the PVdF-HFP membrane with finger-like structure was prepared. Fig. 1 is a comparison of the SEM images of the upper surface, bottom surface and cross-section of both common commercial PP/PE/PP membrane and PVdF-HFP membranes. From the figure, the pore density of both upper and bottom surfaces of the PP/PE/PP composite membrane is denser than that of as-prepared PVdF-HFP membrane. The mean pore size of the PP/PE/PP composite membrane is ca. 26 nm, which is smaller than that for as-prepared PVdF-HFP membrane with a value of 49 nm. Importantly, the PVdF-HFP membrane shows a quite different finger-like cross-section structure with the straight

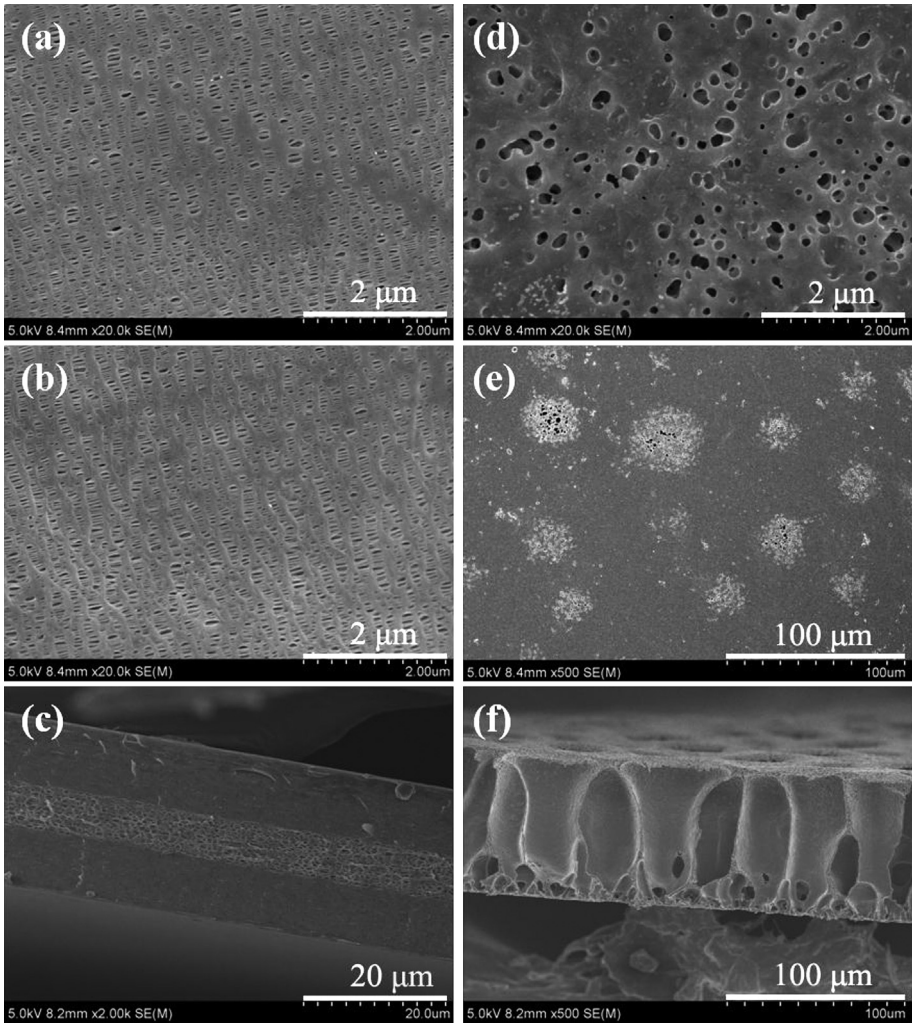

Fig. 1. SEM images of two different porous membranes. (a) and (d) Stand for the upper surface, (b) and (e) the bottom surface, (c) and (f) the cross-section of the commercial PP/PE/PP membrane (left side) and the PVdF-HFP membrane (right side), respectively.

porous paths, which might be beneficial for the Li^+ ion transport across the separator.

Fig. 2 shows the discharge–charge curves of the Li–O_2 batteries with two different separators at the current densities of 0.1 and 5 mA cm^{-2}, respectively. From Fig. 2A, at a current density of 0.1 mA cm^{-2}, the Li–O_2 battery with the PVdF-HFP separator shows a slightly lower discharge capacity but a much lower over potential than that with the PP/PE/PP separator. The discharge plateau of the Li–O_2 batteries with the PVdF-HFP separator is higher than that using PP/PE/PP composite separator by 150 mV. While the charge

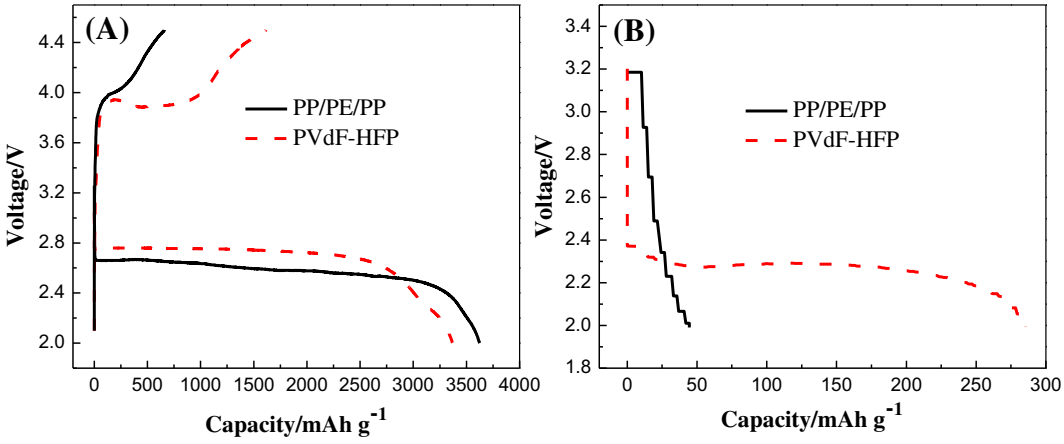

Fig. 2. Discharge and charge curves of the Li–O_2 batteries with two different separators at the current densities of 0.1 (A) and 5 mA cm^{-2}(B), respectively.

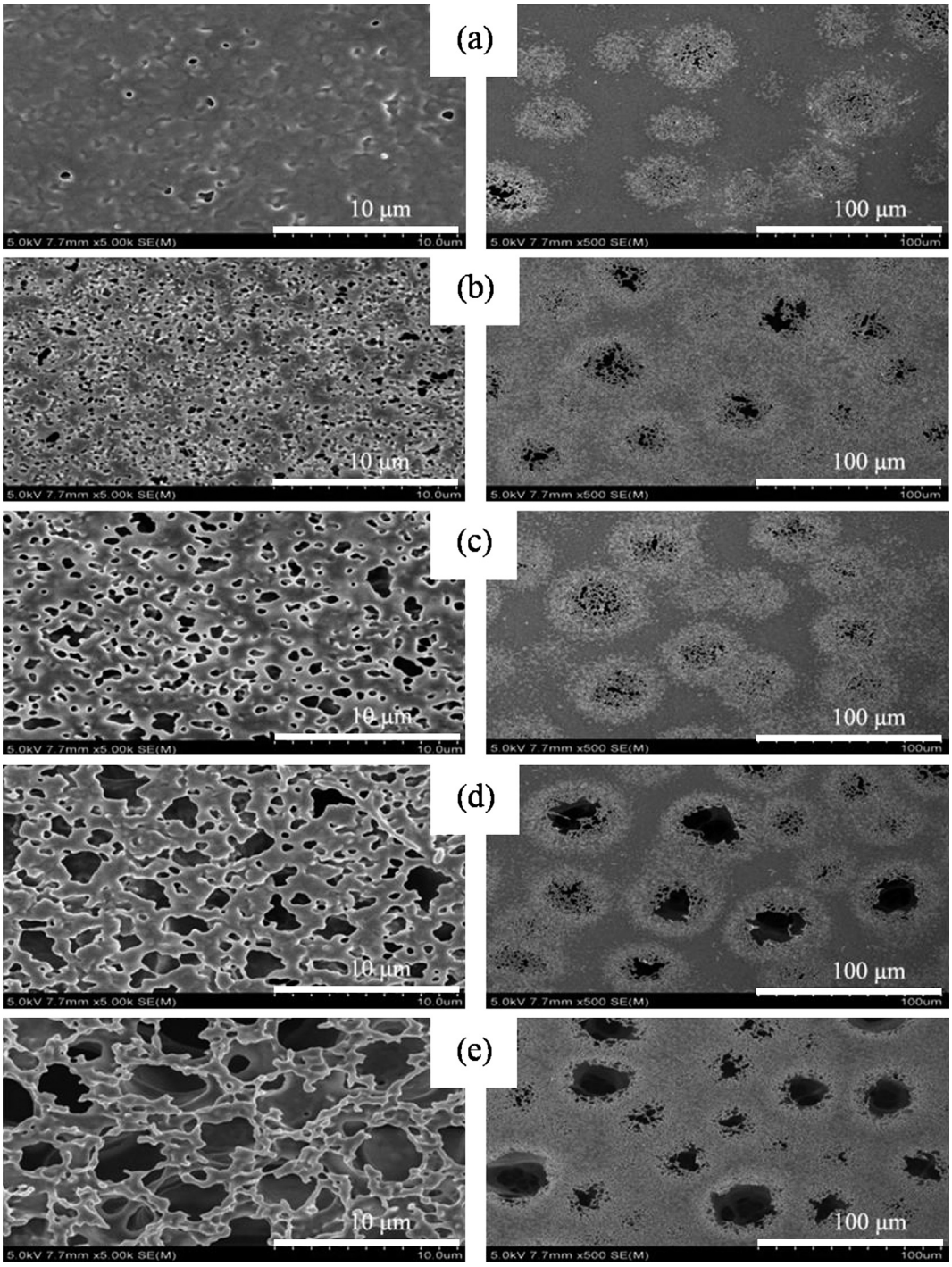

Fig. 3. SEM images of the PVdF-HFP membrane with different pore size and pore density. Left row is upper surface and right row bottom surface; both pore size and pore density increase from a to e.

plateau of the Li—O_2 battery using PVdF-HFP separator is substantially lower over 100 mV. The increased Li^+ transport rate and low membrane resistance could be responsible for the low over potential when using the PVdF-HFP membrane. The Li—O_2 battery using PVdF-HFP membrane as separator is also found to have a higher round-trip efficiency than that using PP/PE/PP composite membrane. With the increase in discharge current, the ohmic polarization would be more serious, the battery discharge voltage decreased rapidly. Due to its higher discharge plateau, the application of PVdF-HFP membrane as separator may improve the rate performance of the Li—O_2 batteries. As expected, the discharge capacity of the Li—O_2 battery with PVdF-

Table 1
The plasma condition and properties of the PVdF-HFP membranes.

Sample	Plasma condition[a]	Mean pore size (μm)	Average thickness (μm)	Absorbency (%)	Ionic conductivity ($\times 10^{-3}$ S cm^{-1})
a	No	0.0497	79.8	400.2	1.81
b	300 W/5 min	0.191	81.2	370.3	1.85
c	300 W/8 min	0.494	78.3.	360.2	2.82
d	300 W/10 min	1.48	81.7	353.6	3.09
e	300 W/12 min	1.99	82.4	339.9	3.11

[a] The plasma condition only contains the O-plasma treatment condition and after that all the membranes were treated by Ar-plasma at 45 W for 10 min.

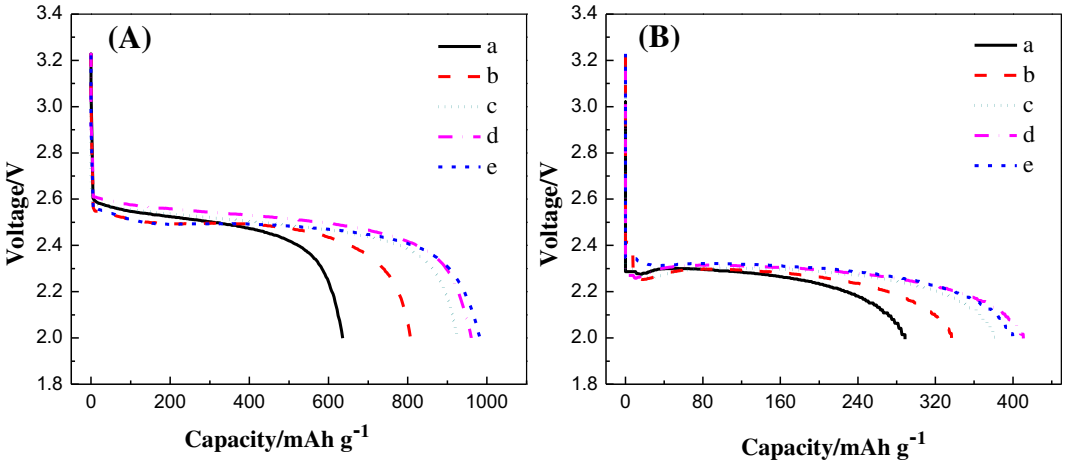

Fig. 4. Discharge curves of the Li–O_2 batteries with different surface pore size and pore density of the PVdF-HFP membrane as separator at the current densities of 1 (A) and 5 mA cm^{-2} (B), respectively. The surface pore size and pore density of the membrane increases from a to e.

Table 2
Thickness, mean pore size and absorbency of the PVdF-HFP membranes with different thickness.

Sample	Average thickness (μm)	Mean pore size (μm)	Absorbency (%)
f	52.2	1.86	352.5
g	78.8	1.48	353.6
h	110.0	1.63	382.9
i	135.4	1.81	400.2
j	170.1	1.33	402.6
k	200.8	1.52	404.3

The membranes were treated by O-plasma at 300 W for 10 min and Ar-plasma at 45 W for 10 min.

HFP separator at a current density of 5 mA cm^{-2} is much higher than that with PP/PE/PP separator as can be seen in Fig. 2B.

To further assess the effects of the pore structure of the membrane on the capacity and rate performance, the PVdF-HFP membranes with different pore sizes and pore densities were prepared. SEM images in Fig. 3 illustrate the morphology of the PVdF-HFP membranes with different pore sizes and pore densities. From the images, the change of the pore size and density of the PVdF-HFP membranes can be observed clearly. Table 1 summarizes the primary information of a series of PVdF-HFP membranes with different pore sizes and pore densities and at a similar thickness range of 78.3–84.1 μm. The ionic conductivities of the PVdF-HFP polymer composite electrolytes measured by a.c. impedance are also listed in Table 1. The ionic conductivity of common PP/PE/PP membrane (plus the electrolyte) is ca. 3.65×10^{-5} S cm^{-1}, which is lower by at least one order of magnitude than that of the parent electrolyte [22]. It is clear that the ionic conductivities of the PVdF-HFP polymer composite electrolytes are much higher than that of common PP/PE/PP electrolytes. The ionic conductivity of the PVdF-HFP polymer composite electrolyte increases with the pore size and reaches a plateau of ca. 3.11×10^{-3} S cm^{-1}. These results clearly indicate that tuning the pore structure of the membrane can improve the ionic conductivity of composite electrolytes, which could be beneficial to a fast Li^+ transport across the membrane.

Fig. 4 illustrates the effects of the membrane's surface pore size and density on the initial discharge capacity of the Li–O_2 batteries at discharge current densities of 1 and 5 mA cm^{-2}, respectively. When the batteries are discharged at a current density of 1 mA cm^{-2} (cf. Fig. 4A), the discharge capacity increases significantly with membranes' pore size, and the highest discharge capacity of ca. 982.4 mAh g^{-1} is observed. From Fig. 4B, at 5 mA cm^{-2}, the discharge capacity increases with the pore size and then reaches a plateau of 410.8 mAh g^{-1} at a mean pore size of 1.48 μm. The

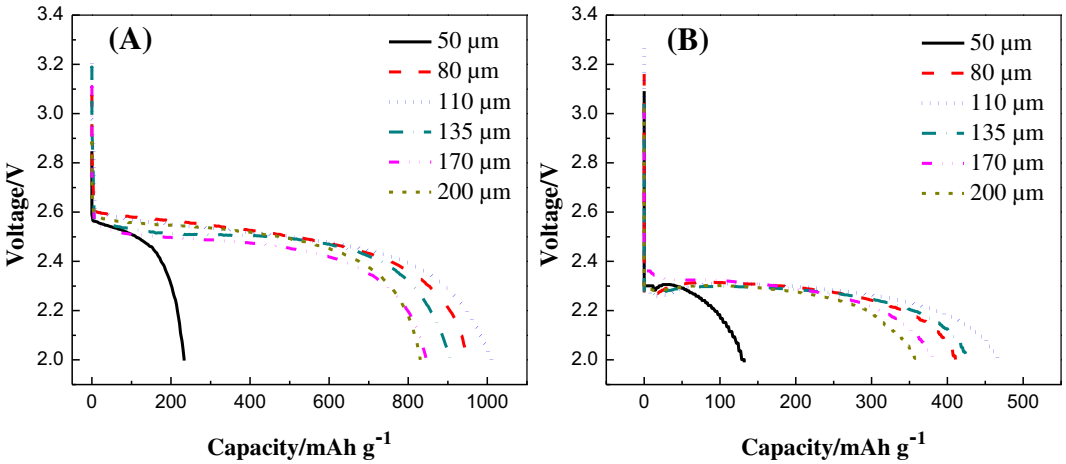

Fig. 5. Discharge curves of the Li–O_2 batteries with different thickness of the PVdF-HFP membrane as separator discharged at the current densities of 1 (A) and 5 mA cm^{-2} (B), respectively.

variation in trends corresponds to the conductivity results listed in Table 1, thus suggesting that the surface pore size and density have a significant effect on the performance of the Li–O_2 batteries because the pore size of the membrane could directly influence the transfer rate of Li^+ ions.

The thickness effects of the PVdF-HFP membrane on the capacity and rate performance of the Li–O_2 battery were further explored. Some fundamental physical properties of a series of membranes with different thicknesses and similar mean pore sizes are listed in Table 2. The absorbance capacity increases with the membrane's thickness. The discharge curves of the Li–O_2 batteries using the PVDF-HFP membranes with different thicknesses at the current densities of 1 and 5 mA cm^{-2} are depicted in Fig. 5. From Fig. 5A, the Li–O_2 battery with the PVdF-HFP membrane of 110 μm exhibits the highest discharge capacity of 1010.0 mAh g^{-1}, at a discharge current of 1 mA cm^{-2}. The same tendency is also observed at a discharge current of 5 mA cm^{-2} (Fig. 5B). The results show a volcano profile with the highest discharge capacity of 466.1 mAh g^{-1} at a membrane thickness of 110 μm. This performance should be a synergistic effect of electrolyte content and Li^+ ion transfer rate.

Based on our optimized results on the PVdF-HFP membrane, Fig. 6 shows a comparison of discharge curves of the Li–O_2 batteries with two different separators. The discharge capacity of the Li–O_2 batteries with the PVdF-HFP separator at the current densities of 1 and 2 mA cm^{-2} is ca. 3 times higher than that with the PP/PE/PP. When discharged at 5 mA cm^{-2}, the initial discharge capacity of the Li–O_2 battery with the PVdF-HFP separator is 466.1 mAh g^{-1}, which is about 10 times higher than that with PP/PE/PP separator. Such a discharge capacity is also much higher than that for the Li–O_2 battery using mesoporous β-MnO_2/Pd air electrode at the current density of 5.1 mA cm^{-2}, which only showed the discharge capacity of 93 mAh g^{-1} [23].

In order to clarify the reason for the better rate performance of the Li–O_2 batteries with the PVdF-HFP membrane, the lithium ion transport number was measured and electrochemical impedance spectroscopy was used to evaluate the electrochemical characteristics of the batteries with two different separators. The measured Li^+ transport numbers of the optimized PVdF-HFP and the PP/PE/PP with electrolyte are 0.292 and 0.262, respectively. The slightly higher Li^+ transport number of the PVdF-HFP polymer composite electrolyte suggests a higher Li^+ transport ability and lower concentration gradient during charge and discharge process which would be benefit for the improvement of rate performance and power density. Fig. 7 shows typical Nyquist plots at the open-circuit voltage for the Li–O_2 batteries using two different separators together with fitted curves based on an equivalent circuit model, shown as insert. The marked points are the experimental data, while the solid lines are the fitted curves. All plots exhibit a semicircle at high frequencies corresponding to the charge-transfer resistances and a linear tail at low frequencies which is related to the diffusion process of Li ions and oxygen in the cathode [24,25]. The physical meanings of each element employed in the equivalent circuit model are as follows:

(1) R_e represents the ohmic resistance, which corresponds to the intercept on the real axis at high frequency
(2) R_{int} is the interfacial resistance between the electrode and electrolyte [26,27]
(3) C_{int} is the capacitance of interface between the electrode and electrolyte
(4) R_{ct} denotes the charge-transfer resistance of the Li–O_2 battery reaction

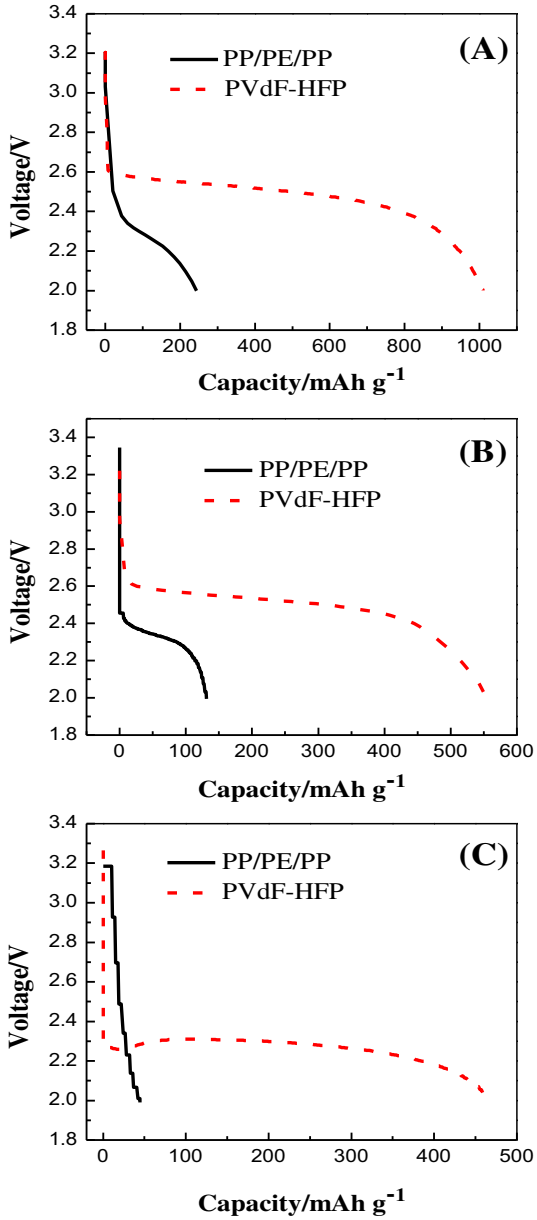

Fig. 6. Discharge curves of the Li–O_2 batteries with two different separators at the current densities of 1 (A), 2 (B) and 5 mA cm^{-2} (C), respectively.

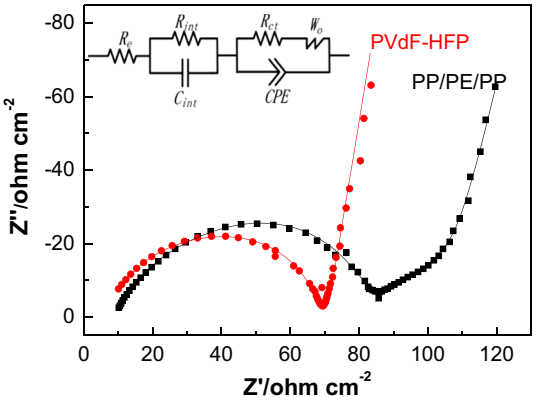

Fig. 7. Impedance spectra of the Li–O_2 batteries with two different separators and the equivalent circuit for fitting the experimental spectra as insert. Symbols denote experimental values, while the solid lines represent the fitted data.

Table 3
Fitted equivalent-circuit parameters of the Li–O_2 batteries with two different separators.

Separator	R_e (Ω cm^{-2})	R_{int} (Ω cm^{-2})	C_{int} (F cm^{-2})	R_{ct} (Ω cm^{-2})	W_o (Ω cm^{-2})	CPE-T (F cm^{-2})	CPE-p
PP/PE/PP	8.85	21.12	1.13×10^{-5}	52.22	71.57	2.23×10^{-5}	0.72
PVdF-HFP	6.20	16.24	2.68×10^{-5}	45. 12	9.16	2.20×10^{-5}	0.78

(5) W_o is the is the finite length Warburg (open-circuit terminus) contribution which relates to the diffusion of Li^+ ions and oxygen to the cathode
(6) CPE (constant phase element) is used to replace ideal capacitor, which is commonly found in conventional equivalent circuit model, to account for the non-uniform structure of the related electrode section.

A very good agreement between the experiment data and simulated results reveals the model's validity. The fitted values for the elements of the batteries with two separators are listed in Table 3. It is clear that the battery with the PVdF-HFP separator exhibits the lower values of R_e, R_{int}, R_{ct} and W_o than that with the PP/PE/PP separator. A lower R_e suggests a lower membrane resistance of the PVdF-HFP membrane. Lower R_{int}, could be ascribed to the decreased contact resistance between the electrode and electrolyte [26]. The decrease in R_{ct} can explain the enhanced rate performance of the Li–O_2 battery with the PVdF-HFP membrane. While a much lower W_o of the Li–O_2 battery with the PVdF-HFP membrane strongly suggests a faster Li^+ ion transport across the porous membrane, which is attributed to the straight and large pore size of the PVdF-HFP membrane, in good agreement with the ionic conductivity and lithium ion transport number results.

4. Conclusions

PVdF-HFP copolymer membranes with tunable pore size and density were fabricated and used as the separator for the Li–O_2 batteries. The Li–O_2 battery using the PVdF-HFP separators exhibited a significantly enhanced rate performance. Such an improved rate performance is ascribed to a faster Li^+ transport across the PVdF-HFP membrane, which has been verified by a.c. impedance results. The highest discharge capacity of 466.1 mAh g^{-1} was achieved at a discharge current density of 5 mA cm^{-2} for the battery with the PVdF-HFP membrane thickness of 110 μm and pore size of 1.48 μm. Although the cyclability of the Li–O_2 batteries is unsatisfactory, this work still provides a new promising approach to improve the rate performance of the Li–O_2 battery.

Acknowledgments

This work was supported by the National Basic Research Program of China (973 Program, 2012CB932800), the Natural Science Foundation of China (21103220, 21176119), Shanghai Science and Technology Committee (11DZ1200400) and the Knowledge Innovation Engineering of the CAS (12406 and 124091231).

References

[1] J.-J. Xu, D. Xu, Z.-L. Wang, H.-G. Wang, L.-L. Zhang, X.-B. Zhang, Angewandte Chemie International Edition (2013).
[2] J. Xiao, J.Z. Hu, D.Y. Wang, D.H. Hu, W. Xu, G.L. Graff, Z.M. Nie, J. Liu, J.G. Zhang, Journal of Power Sources 196 (2011) 5674–5678.
[3] Z.-L. Wang, D. Xu, J.-J. Xu, L.-L. Zhang, X.-B. Zhang, Advanced Functional Materials 22 (2012) 3699–3705.
[4] A.K. Thapa, S. Tae Ho, S. Ida, G.U. Sumanasekera, M.K. Sunkara, T. Ishihara, Journal of Power Sources 220 (2012) 211–216.
[5] Y. Shao, F. Ding, J. Xiao, J. Zhang, W. Xu, S. Park, J.-G. Zhang, Y. Wang, J. Liu, Advanced Functional Materials (2012).
[6] S.H. Oh, L.F. Nazar, Advanced Energy Materials 2 (2012) 903–910.
[7] Z. Peng, S.A. Freunberger, Y. Chen, P.G. Bruce, Science 337 (2012) 563–566.
[8] L. Zhang, X. Zhang, Z. Wang, J. Xu, D. Xu, L. Wang, Chemical Communications 48 (2012) 7598–7600.
[9] Y.C. Lu, Z. Xu, H.A. Gasteiger, S. Chen, K. Hamad-Schifferli, Y. Shao-Horn, Journal of the American Chemical Society 132 (2010) 12170–12171.
[10] X. Lin, L. Zhou, T. Huang, A. Yu, Journal of Materials Chemistry A 1 (2013) 1239–1245.
[11] H.G. Jung, J. Hassoun, J.B. Park, Y.K. Sun, B. Scrosati, Nature Chemistry 4 (2012) 579–585.
[12] K.M. Abraham, Z. Jiang, Journal of the Electrochemical Society 143 (1996) 1–5.
[13] G. Girishkumar, B. McCloskey, A.C. Luntz, S. Swanson, W. Wilcke, The Journal of Physical Chemistry Letters 1 (2010) 2193–2203.
[14] Y. Tian, H. Yue, Z. Gong, Y. Yang, Electrochimica Acta 90 (2013) 186–193.
[15] Y. Qin, J. Lu, P. Du, Z. Chen, Y. Ren, T. Wu, J.T. Miller, J. Wen, D.J. Miller, Z. Zhang, K. Amine, Energy & Environmental Science (2013).
[16] D. Feng, Y. Lv, Z. Wu, Y. Dou, L. Han, Z. Sun, Y. Xia, G. Zheng, D. Zhao, Journal of the American Chemical Society 133 (2011) 15148–15156.
[17] W. Hui, X. Kai, W. Lingyan, H. Yu, Journal of Power Sources 219 (2012) 263–271.
[18] H. He, W. Niu, N.M. Asl, J. Salim, R. Chen, Y. Kim, Electrochimica Acta 67 (2012) 87–94.
[19] W. Pu, X. He, L. Wang, C. Jiang, C. Wan, Journal of Membrane Science 272 (2006) 11–14.
[20] W. Xu, J. Hu, M.H. Engelhard, S.A. Towne, J.S. Hardy, J. Xiao, J. Feng, M.Y. Hu, J. Zhang, F. Ding, M.E. Gross, J.G. Zhang, Journal of Power Sources 215 (2012) 240–247.
[21] J.G. Zhang, D. Wang, W. Xu, J. Xiao, R.E. Williford, Journal of Power Sources 195 (2010) 4332–4337.
[22] J.Y. Song, Y.Y. Wang, C.C. Wan, Journal of the Electrochemical Society 147 (2000) 3219–3225.
[23] A.K. Thapa, Y. Hidaka, H. Hagiwara, S. Ida, T. Ishihara, Journal of the Electrochemical Society 158 (2011) A1483.
[24] P. Kichambare, J. Kumar, S. Rodrigues, B. Kumar, Journal of Power Sources 196 (2011) 3310–3316.
[25] J. Kumar, S.J. Rodrigues, B. Kumar, Journal of Power Sources 195 (2010) 327–334.
[26] M. Mirzaeian, P.J. Hall, Journal of Power Sources 195 (2010) 6817–6824.
[27] M. Eswaran, N. Munichandraiah, L.G. Scanlon, Electrochemical and Solid-State Letters 13 (2010) A121.